# Improvement of spectral indicators for intermittent cyclic signals with application to bearing faults for wind turbine monitoring

Adrien Marsick, Hugo André, Ilyes Khelf, Quentin Leclere, Jérôme Antoni

# Improvement of spectral indicators for intermittent cyclic signals with application to bearing faults for wind turbine monitoring

**A. Marsick** [1,3], **H. Andre** [2], **I. Khelf** [3], **Q. Leclere** [1], **J. Antoni** [1]
[1] Univ Lyon, INSA Lyon, LVA, EA677,
69621 Villeurbanne, France

[2] Univ Lyon, UJM Saint Etienne, LASPI, EA 3059,
42334 Roanne, France

[3] Engie Green,
34967 Montpellier, France

## Abstract
Spectral indicators for the monitoring of rotating machinery assume continuously and steadily observable cyclic fault signature. Specific types of faulty ball bearings generate intermittent fault signature and are improperly monitored by classical techniques. A model of intermittent cyclic signal is built. Based on the intermittence function, an improved spectral indicator is proposed. A method of blind estimation of the intermittence function is given with application to the surveillance of a damaged ball bearing of an industrial wind turbine.

## 1 Introduction

The surveillance of rotating machinery is a major challenge to implement a cost-effective maintenance strategy, improving safety and lowering the environmental impact of industrial activities. The presence of a fault can modify the temperature of the machine [1], impact the lubricant [2], or the vibration generated by the operating machine [3]. The latter is the most common technique in use and enjoys several dedicated methods and sensors. Modern vibration-based condition monitoring of rotating machinery relies on signal processing tools built on the framework of the cyclostationarity theory [4]. These techniques are widely used for industrial applications but rely on the key assumption of stationary operating conditions. In fields such as wind power, the efficiency of condition monitoring is undermined by the variability of speed and load conditions. However, an appropriate hidden law may exist that restores its cyclostationarity properties. For instance, the speed nonstationarity has been partially resolved by the new class of angle-time cyclostationarity [5]. In this case, appropriate order tracking with the use of instantaneous frequency of a shaft restores the cyclic properties. Yet, the application of these tools is limited to continuously and steadily observable phenomena. In particular, signals where the fault signature is intermittent are unsuitably monitored by such techniques. Intermittent faults are controlled by a binary external variable that affects the local expression of the fault cyclic energy flow. Unlike speed nonstationarity, this uncontrolled variable is not locked to particular operating conditions. A practical example of intermittency would be a flaked ball rolling element in a bearing. Due to the self-rotation of the ball within the cage, the flake is not necessarily moving in the two-dimensional plane that contains the races.

There is a need to develop appropriate signal processing tools to deal with intermittent fault signatures. An original approach based on the short-time properties of the signal is presented. The method aims at finding the optimal window that silences the uninformative portions of the signal to create an appropriate weighted spectral indicators. Short-time portions of the signal are ranked and the weighting strategy is

achieved by using the fact that the progressive addition of new informative portions should leave the Fourier coefficients related to the cyclic signature unchanged. The method achieves a trade-off between spectral resolution and peak emergence in the spectrum and does not degrade the monitoring capacities for signals with non-intermittent faults. Along with numerical examples, the method is applied to industrial signals from a damaged wind turbine bearing with defective rolling elements, proving its efficiency for complex signals. This original approach to handle intermittent cyclic signals is likely to provide earlier detection and better fault severity estimation by reducing the variability caused by intermittency.

# 2 Cyclic spectral indicators for bearing faults

## 2.1 From broadband to narrowband scalar indicators

The vibration received by a sensor is a complex mixture of sources distorted by transmission path, with often a weak fault signature. The different sources distinguish from one another by their periodic statistical properties. The critical components to monitor (e.g. gears, bearings, shafts...etc.) generate forces synchronous with the rotation of a kinematic element of the machine. Such sources have been largely described by the cyclostationary theory [4, 6] defined by a hidden periodicity of their statistical properties. Such periodicity is not necessarily obvious for signals described as a function of time but can be restored by an angular variable linked to a rotation of the machine. For instance, the periodicity of gears signals is better described with an angular variable of shaft rotation than time, with insensitivity to variations of the instantaneous rotation. Scholars have focused on developing techniques dedicated to angular approaches such as order tracking to numerically change the observation variable so as to restore the periodicity of the faulty source. The fault signature might feature a periodic waveform, like gear or unbalanced shafts signals, or a periodic flow of energy for bearing faults or combustion signals. Knowing the rotation speed and the geometric properties of the component to monitor allows to pinpoint specific frequencies associated with possible faults. Expert approaches with dedicated methods based on vectorial (Fourier spectrum, synchronous average) or matricial (spectral correlation, angle-time framework) representations allow fine diagnostic and estimation of the health of the machine. However, when it comes to monitoring a fleet of machines, there is a need to create scalar fault-sensitive indicators [7]. Global indicators monitoring the broadband level of vibration (RMS) or the sparsity of the signal (peak-to-peak, kurtosis) allow a first estimation of the condition of the machine but rarely localise the fault or focus on a precise phenomenon. The goal for automation is to extract a scalar indicator from the vectorial representation that would be sensitive to one type of fault only. A common way to monitor specific components is to build spectrum amplitude-based indicators that takes the value of a peak in a narrowband around the expected frequency of the fault. However, all these scalar indicators assume a continuously and steadily observable cyclic signature. This assumption does not hold for specific types of bearing fault signatures.

## 2.2 The specific fault signature of a flaked ball

Rolling elements bearing are described by a few geometric quantities such as pitch diameter $D$, rolling element diameter $d$, load angle $\alpha$, and the number of rolling elements $Z$ as shown schematically in Fig. 1. Incipient faults of rolling element bearings are characterised by a local loss of material either on the races or on the rolling elements. When operating, a train of impulses is generated by the interaction between the spall and a matting surface. The inter-impact duration depends on the type of damaged element and the rotating speed of the races. Considering that the contact angle is the same for every rolling element and assuming perfect rolling conditions, the motion of each element can be derived. From it, theoretical values of key cyclic frequency of a faulty bearing (BPFO, BPFI, BSF, FTF) give the expected duration of fault signature, as presented by Howard [8].

Modern monitoring of rolling elements bearing is thus based on the expected periodicity of the statistical properties of a specific fault signature. As described by Randall and Antoni [9], the fault signature of rolling bearing is well modeled by cyclostationarity at the second order. Hence, envelope angle spectrum or spectral correlation are recommended quantities for diagnostic. Dedicated scalar indicators are designed to monitor

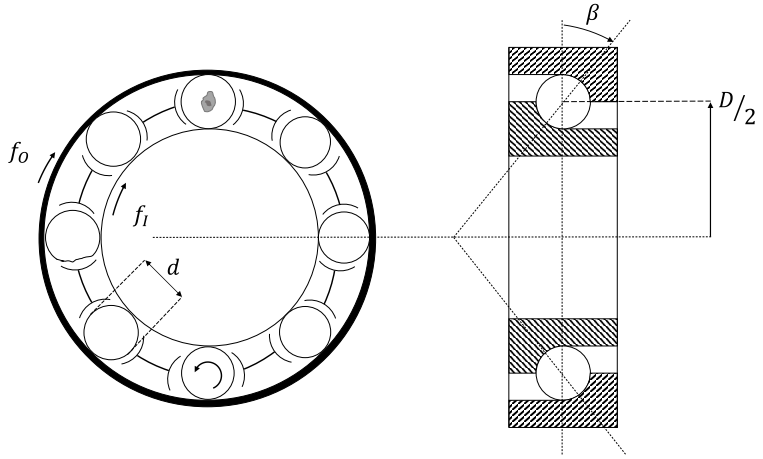


Figure 1: Schematic of a ball bearing. Two flaked balls are drawn at 9 and 12 o'clock.

narrow frequency bands of the signal expected to be fault-sensitive. A simple way to do so is to take the maximal amplitude within a small band around the expected fault frequency in a spectrum. The efficiency of the indicator lies in the intrinsic assumption that the peak amplitude is correlated with the gravity of the fault.

However, using the ball spin frequency to monitor the health of the rolling elements assumes that the flake does not leave the ball perimeter rolling between the races. When it comes to ball bearings, there is no reason why the spin rotation of the ball would be contained in a two-dimensional plane, due to the combination of axial and radial load, slippage and the impacts with the spall [10, 11]. As shown schematically in Fig. 1, the ball located at 9 o'clock will generate a train of cyclic impulses complying with the BSF periodicity, but not the 12 o'clock ball as it is not interacting with a mating surface. For a short period of observation, the train of impulses can be either completely absent, continuously present, or intermittent. Fig. 2 presents an experimental example of vibration signal with an intermittent signature from a rolling bearing with flaked balls. During the 10 s of recording, the train of impulses is present during the first second and reappears between 5 s and 7 s. Here, signal-to-noise ratio is strong enough for the cyclic signature to emerge visually but some cases would require a short-time spectral approach to reveal the intermittency.

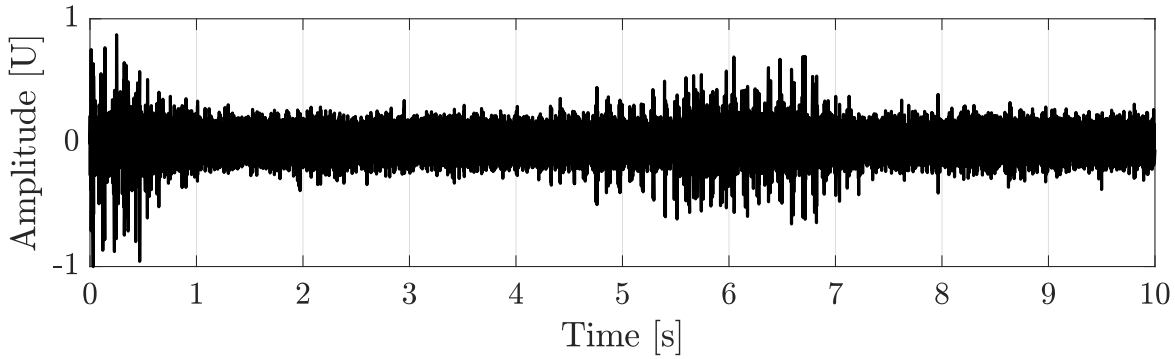


Figure 2: Vibration signal recorded from a ball bearing with flaked rolling elements. The signal is part of the data set of section 5.

# 3 Binary intermittence and classical indicators

## 3.1 Model of binary intermittence

There is a need to define a model of intermittence for these types of fault signature. Let $C_{\alpha_0}(\theta)$ be a cyclostationary phenomenon. It bears a periodicity of frequency $\alpha_0$ with respect to the angular variable $\theta$. Let $\zeta(t)$ be a binary variable controlling the cyclostationary signature appearance. The corresponding model would be

$$x(t) = \zeta(t) \times C_{\alpha_0}(\theta(t)) + \epsilon, \zeta \in \{0; 1\} \tag{1}$$

where $\epsilon$ is a noise term. As an illustrative example, Fig. 3 presents an intermittent sinusoidal signal where the binary variable $\zeta$ is represented in black dotted lines. In the proposed model, the intermittence law $\zeta$ is chosen as a variable that does not exhibit any cyclic properties, the latter being already covered by the cyclostationary source $C_{\alpha_0}(\theta(t))$. Two close cases fall into this latter category of angle-driven intermittence. First, cyclostationary signals can incorporate intrinsic short-time intermittency of the waveform. For example, the train of impulses generated by a faulty bearing is an intermittent flow of energy locked to an angular variable. Second, periodic modulations of the amplitude of the cyclic waveform will look like the intermittency described in the model of Eq. (1), but are still locked to an angular variable. In this case, it would lead to the creation of sidebands in the spectrum with still a clear possibility to assess the intensity of the phenomenon.The intermittence of the proposed model drives global observability of the waveform independently of the angular variable.

A few assumptions on the physical model are made herein. First, the controlling variable is strictly binary so applicable to limited speed and load non-stationary conditions. Then, the binary variable acts as a switch, so two separated clusters of impulses during an observation time are supposedly still coherent. When working on intermittent signals generated by flaked balls on a roller bearing, there is no physical reason why the new train of impulse would recover its exact previous phase.

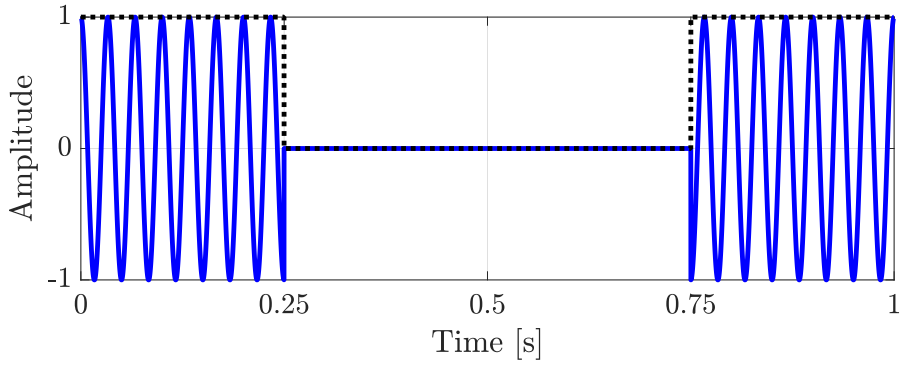


Figure 3: Intermittent sinusoidal signal (blue solid line) with intermittence function $\zeta$ (black dotted line) .

## 3.2 Insufficiency of classical spectral indicators

Whether it readily comes in the raw signal or after processing steps, the intermittent cyclic signature will eventually appear at some point in the form of a harmonic analytical signal of frequency $\alpha_0$ with added noise such as:

$$x[n] = \zeta[n]A[n]e^{j(2\pi n\frac{\alpha_0}{F_s}+\phi)} + \epsilon[n], \tag{2}$$

where $x[n]$ is a sampled signal acquired at the sampling frequency $F_s$ and $n$ is the sample index, $\phi$ the initial phase and $\epsilon$ a noise term supposed normally distributed. The scaled discrete Fourier transform $X(f)$ of a

signal $x[n]$ of $N$ samples with a sampling frequency $F_s$ is

$$X(f) = \frac{1}{\sum_n w[n]} \sum_{n=0}^{N-1} w[n]x[n]e^{-j2\pi n \frac{f}{Fs}}, \tag{3}$$

where the signal is weighted by a window function $w[n]$. If the signal comprises a cyclic component rotating at the frequency $\alpha_0$, it will be the only one to demodulate to the amplitude phasor $A[n]$ rather than zero

$$X(\alpha_0) = \frac{1}{\sum_n w[n]} \sum_{n=0}^{N-1} w[n] \left(\zeta[n]A[n]e^{j\phi} + E[n]\right), \tag{4}$$

with $\sum_n E \sim O(\sqrt{N})$. The classical Fourier analysis gives the same importance to each sample that is $w[n] = 1/N$. As such, the noise contribution in Eq. (4) will scale as $1/\sqrt{n}$ . For a continuously and steadily observable phenomenon ($\zeta = 1, \forall n$ and A is constant) the Fourier coefficient accurately returns the amplitude coefficient $A$. However, when the signature is intermittent, the average operation of the Fourier transform will give the same weight to samples with the cyclic signature and to the non-informative part of the signal. The amplitude of the corresponding Fourier coefficient will lead to biased estimation. However if one correctly estimates the hidden law that drives the intermittency $\zeta$, the weighting function can be tuned accordingly so to silence the uninformative portion of the record. The optimal case would be $w[n] = \zeta[n]$.

Fig. 4 presents the Fourier transform of the signal presented in Fig. 3 either with uniform weight or weighted with the intermittency function. The signal being present half of the time, an amplitude-based indicator would be biased and return half of the amplitude of the sinusoidal. With the weighted version of the Fourier transform, the uninformative part of the signal is ignored and the amplitude is correctly returned. The silenced portion of the signal only acts like zero-padding.

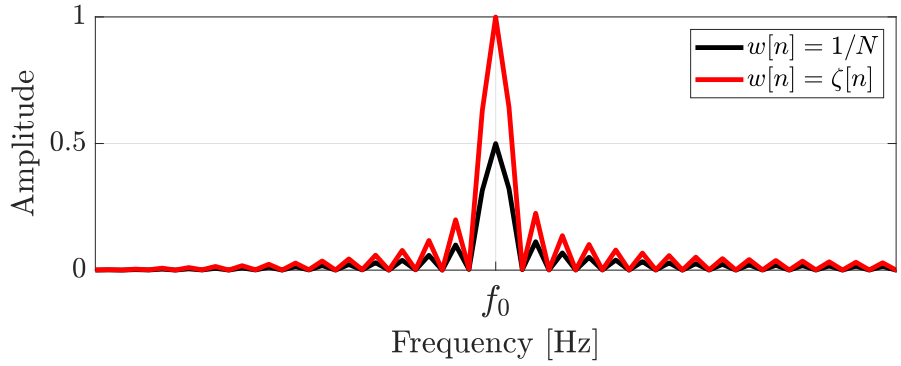


Figure 4: Fourier transform of the signal of Fig. 3 with a uniform weight (black line) and weighted by the intermittence function (red line).

# 4 Blind estimation of the weighting function

## 4.1 Existing approaches and the necessity of fine selection of informative zones

There is a need to estimate the function driving the intermittence from the signal itself. The selection of informative parts in signals has been thoroughly studied for speech recognition applications [12, 13]. These approaches model the signal as a mixture of components with latent variables. The signal is converted into a sequence of non-negative spectral vectors to find the intermittence law. The decomposition does not take advantage of the expected cyclic frequency of the train of impulses and does not apply for cases of continuously observable signatures. The clustering of spectrograms has been applied to bearing monitoring applications

using different techniques such as non-negative matrix factorization [14], hierarchical clustering [15] or hidden Markov models [16]. These techniques work well to highlight the angle locked short-time intermittence of the train of impulses but face difficulties for the type of intermittence described in this work. First, splitting the signal into short segments reduces the resolution in the frequency domain. Concurrent cyclic events with near frequencies can hinder the ability to focus on a single type of phenomenon. On the other hand, a longer short-time segment would also lead to a too coarse time resolution for the intermittence law. Alternatively, focusing on the instantaneous envelope of narrowband signal around the expected fault frequency would be very prone to noise contamination and unsuitable. Concurrently to finding the intermittence law, another approach for intermittence insensitive scalar indicators would be to retain only a fixed proportion of the signal. For example, a scalar indicator would be to select the maximum peak amplitude in a set of short-time Fourier transform. These kinds of selection would systematically throw away portions of the signal even if they were informative. It would also be more sensitive to bursts of broadband noise as it would retake only the strongest energy.

The goal of the proposed method is to retain as much informative part as possible so as to achieve a trade-off between spectral resolution and peak emergence in the spectrum. In this way, the method should not degrade the capacities for non-intermittent signals.

## 4.2 Proposed method of blind estimation

The principle of blind estimation of the intermittency function is based on differentiated convergence of harmonic and noise signals with increasing observation time in Eq. (4). By playing with the global observation window $w$, more and more equivalent samples $N$, not necessarily consecutive, are taken into account. As long as added segments contain a harmonic component, the Fourier transform will demodulate to a fixed amplitude phasor $A$. If a segment with only noise is added, the corresponding spectral amplitude will decrease. The break of slope will indicate the estimation $w$ of the intermittence function $\zeta$. The flowchart of the method is presented in Fig. 5. First, the signal is split into segments with possible overlap and local windowing to avoid spectral leakage. The Fourier transform of each segment is calculated and the segments are ranked according to the peak amplitude of interest. As developed in Appendix A, the sum of zero-padded complex spectra is equivalent to a global window applied on the signal before transformation to the spectral domain. Since the manipulation of the global window is easier with this formulation, it will be preferred in what follows. Then, based on the ranking, the complex spectra are progressively added, which is equivalent to an increasing observation window. Finally, the amplitude of the expected peak is tracked for each spectrum and studied as a function of the total number of samples taken into account. Any break on the slope would mean that the next portions of signal added do not contain the cyclic signature. A general recommendation for the initial short-time Fourier transform would be to choose a window long enough to cover multiple periods of the targeted cyclic event with a fine overlap to ensure a sufficient time resolution for the intermittence estimation.

Getting back to the signal of Fig. 3, the method would go as schematically shown in Fig. 6 assuming one has a correct segment ranking estimation. First, segments up to 0.25 s are added, and the spectral amplitude of the analytical signal would be correctly estimated, since all the segments contain cyclic information. Then, the part of the signal between 0.75 s to the end is taken into account with still no effect on the amplitude of the target peak. Eventually, all the informative portions of the signal would be incorporated and the segments between 0.25s and 0.75s would be added. Containing no cyclic component, the Fourier coefficient will progressively decrease to comply with the ratio of informative to noise parts. The estimation of intermittence law is taken as the equivalent global window at the slope break.

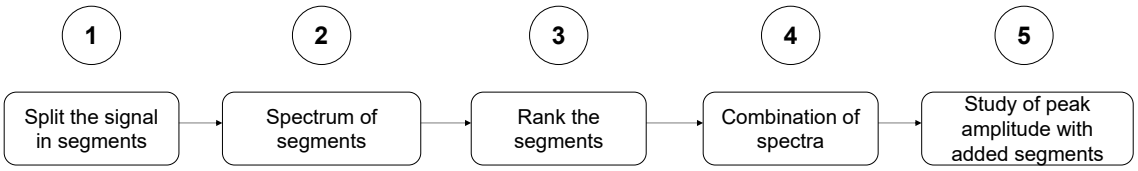


Figure 5: Flowchart of the method for blind evaluation of the intermittence function.

This estimation method bears many advantages. It focuses on a narrow frequency band around the expected cyclic frequency yielding a relative insensitivity to other cyclic events. Using the progressive addition of complex spectra allows a trade-off between spectral resolution and noise contamination. Using overlapping segments permits a fine time resolution for the estimation of the intermittence. Since the stopping criterion is based on a slope analysis, it does not select a fixed proportion of the signal and will retain all the signal for continuously and steadily observable cyclic signatures. However, the method is still limited to classes of binary intermittence and the first estimation for the ranking of the segments is crucial.

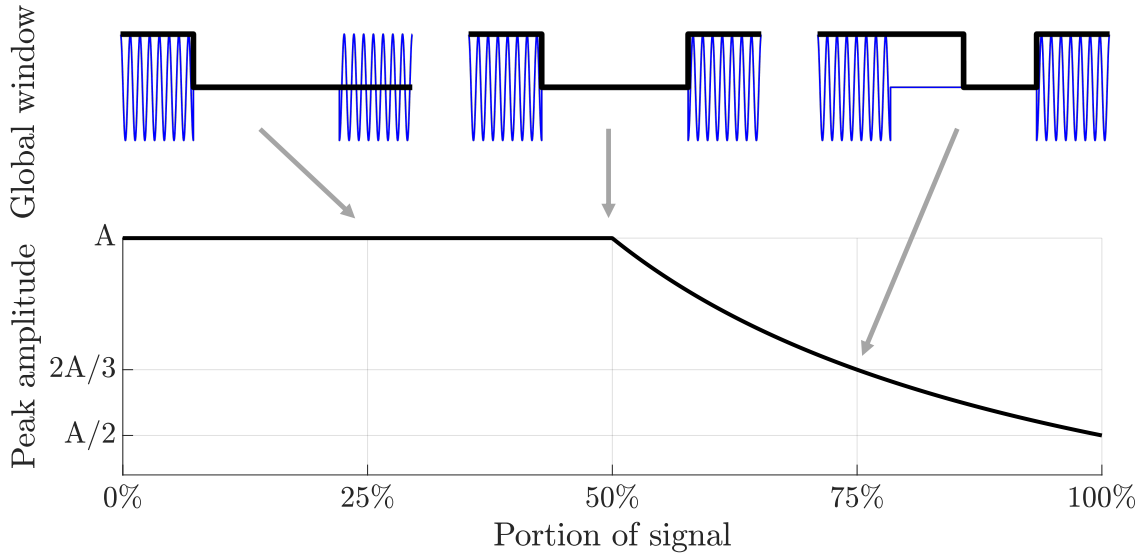


Figure 6: Schematic example of the method based on the intermittent signal of Fig. 3. The evolution of the amplitude-based spectral indicator is shown on the bottom with equivalent windows in the top.

# 5 Experimental validation on industrial application

## 5.1 Presentation of the system

The proposed approach is tested on the data from an industrial wind turbine of 2MW. An accelerometer is placed in the vicinity of the bearings supporting the high-speed shaft (HSS) in the generator and records associated vibration signals during the normal operation of the machine. All the signals are recorded during 10 s sampled at 20 kHz, and quantified with a 12 bits resolution. To limit the effect of varying loading, the signals are recorded for similar operating conditions. The signals are not recorded with a constant inter-time interval due to dependency to external wind conditions. One of the bearings supporting the high-speed shaft in the generator was closely monitored for a period of three months. The model is a 6330 SKF bearing with fault frequencies of $BSF = 2.365 f_{\mathrm{HSS}}$ and $FTF = 0.399 f_{\mathrm{HSS}}$. At the beginning of the monitoring period, the signals were already known to exhibit peaks in the spectrum at the ball pass frequency on the outer ring (BPFO). However, with time, peaks localised at the ball spin frequency and higher harmonics appeared in multiple records. During maintenance operation, the bearing was replaced and multiple spalls were found on the outer race. Three rolling elements were also impacted with spalls of around 15 mm diameter for a ball diameter of 50 mm. Fig. 7 presents pictures of the damaged bearing.

For each record, the signal is processed as follows to highlight the signature of the faulty bearing. The band-pass envelope is obtained by filtering it between 5 kHz and 8 kHz. The bandwidth was chosen with a kurtogram approach [17]. The generator produces a harmonic signature at the frequency $f_g = 72 f_{\mathrm{HSS}}$ whose phase demodulated by narrow-band filtering [18] is used for computed order tracking of the envelope. The indicator of fault severity for surveillance is based on the amplitude of the peak of BSF in the angle envelope spectrum.

Figure 7: Rolling elements of the damaged bearing.

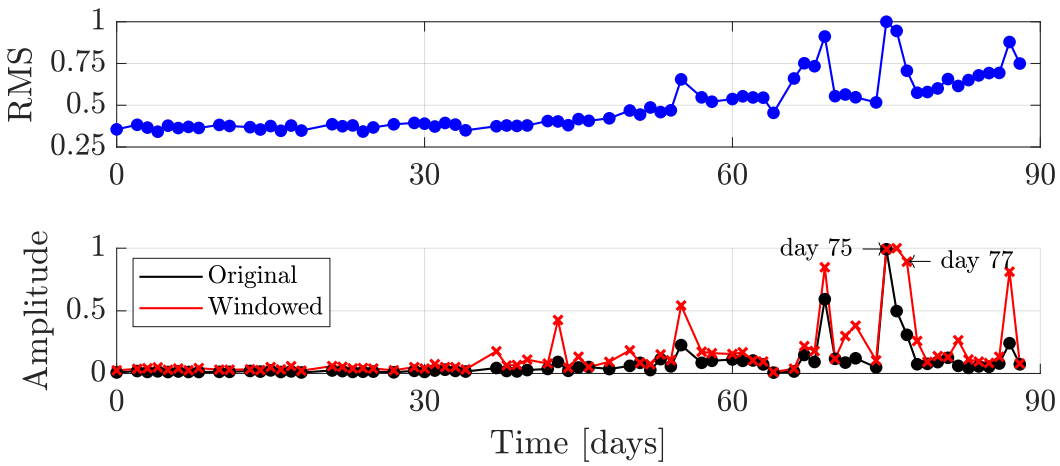


Figure 8: Scalar indicator calculated from 10s vibration acquisition during a period of three months. The root mean square of the signal is presented (top) along with the maximum amplitude of the spectrum within a narrow band around the expected fault frequency (bottom).

## 5.2 Improved scalar indicators with blind estimation of the intermittence law

Figure 8 presents the different scalar indicators calculated during the monitoring period. The RMS of the total signal is presented on the top and amplitude-based indicators are either calculated from the spectrum of the complete signal or the windowed signal shown in the bottom. To monitor the amplitude with accuracy, the local window $g$ is chosen to be a flattop window of length $1/20$ the total number of samples with an overlap of $4/5$ the length of the window. Then, the segments are ranked based on their maximum amplitude in a narrowband around the BSF and progressively added. Along with the amplitude of the BSF, the background noise level is evaluated as the median value of amplitude in a larger band around the expected BSF peak.

The evolution of BSF peak amplitude with increasing signal length is monitored. The data points are smoothed to reduce small variations and the slope is calculated. The global window is taken for the slope of the BSF amplitude being below 80% of the background noise slope. Two consecutive points complying with this condition are required as a stop criterion. The stopping criterion was tuned with a trial-and-error approach.

After approximately a month, both the RMS and the amplitude-based indicators rise, indicating a probable degrading health condition. Some records with the weighted Fourier transform approach are brought out with a strong offset compared to the classical indicators. It certainly signifies that the fault signature is intermittent, so the original indicator is biased by the average operation of the Fourier transform. The signals of day 75 and day 77 are more precisely described. In the signal of day 75, the BSF signature is continuously and steadily observable during the 10 s of recording. On the contrary, the signature of the signal 77, which

was already presented in Fig. 2, is intermittent.

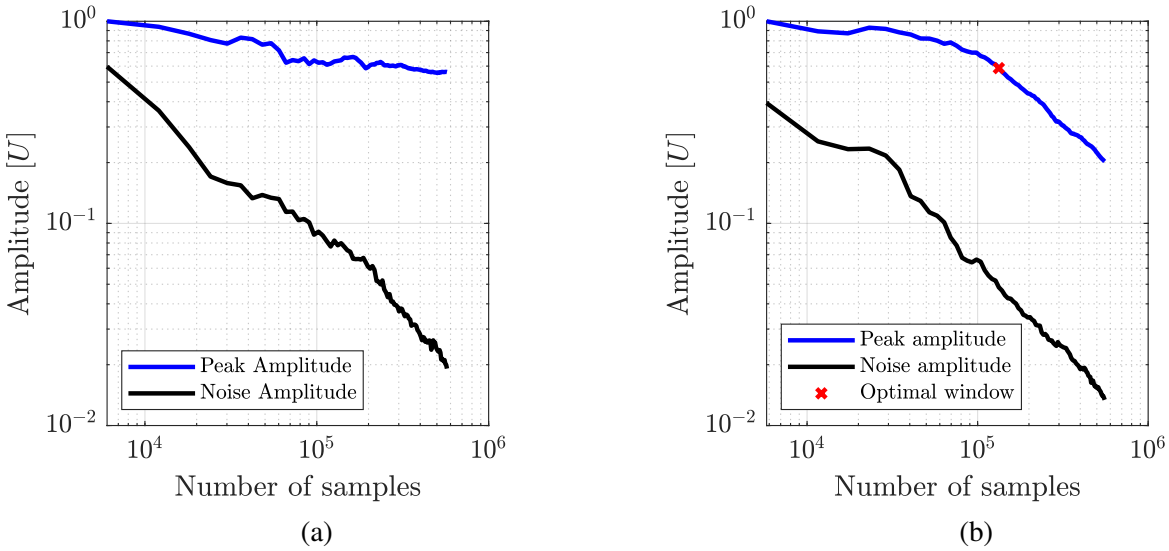


Figure 9: Evolution of the peak amplitude at the BSF (blue line) compared with the noise level (black line) as a function of the number of samples taken in account in the spectrum, normalised to maximum amplitude. The corresponding signals on Fig. 8 are (a) day 75 and (b) day 77.

Figure 9 presents the spectral amplitude at the expected frequency and the background noise level for the signals of day 75 (Fig. 9 (a)) and day 77 (Fig. 9 (b)). For day 75, the peak amplitude slowly decreases and scales as $-0.05$. The noise amplitude scales as $-0.32$. The small decrease in the BSF amplitude can be explained by the combined distribution of instantaneous amplitude and a slight loss of coherence due to slippage. Given the small difference in slope, there is no intermittency so the whole signal is kept as the optimal window.

The case is different for the signal of day 77 (Fig. 9 (b)). The peak amplitude is relatively constant up to $10^5$ samples but then shares the same slope as the noise amplitude. Based on this chart, the optimal window is found at the break of slope, indicated with the red cross. An interesting point to note is that after the red cross, the distance between the peak and noise amplitude is the same. Taking all the signals will not degrade the emergence of the signal from the background noise but hide the true intensity of the cyclic event.

Figures (10-11) present envelope signals of days 75 and 77 (black lines), with the equivalent windowed envelopes given by the method (red lines). Fig. 10 shows that the train of impacts is continuously present which is confirmed by the selection of the entire signal. Data points located at the edges are given less weight due to the effect of the window. More interestingly, Fig. 11 shows the intermittent cyclic signature with strong impulses emerging from the envelope. The method selected in the signal the portions so to maximise the spectral amplitude, excluding the weaker signature between 4.5 s and 5.5 s.

Figure 12 shows the two different envelope spectra of signal 77 from either the whole signal or its intermittent weighted version. The spectra are normalised to maximum amplitude at the BSF peak. Both spectra exhibit the same peaks with different amplitude. The spectrum obtained with the entire signal exhibits a lower background noise floor than the windowed signal. However, the spectral signature of the BSF with associated FTF peaks is more visible and extends to higher harmonics. Despite showing a noisier spectrum, the intermittent weighted spectrum is likely to give a more accurate image of the intensity of the cyclic physical phenomenon at stake.

Getting back to the indicators of Fig. 8, the improved spectral indicators give clearer information about the fault gravity. First, on the early detection between days 30 and 60, some of the improved indicators occasionally separate from the classical indicators. The true intensity of the intermittent fault signature previously hidden by the average operation of Fourier transform is now better rendered in the scalar indicators. From day 60 to 90, the improved indicators show a better separation between different classes. Points of low amplitude are supposedly signals without or with a weak BSF signature. On the other hand, a class of points,

like days 75  77, is now brought out and is supposed to be more representative of the gravity of the spalls. The method takes off part of the bias of intermittence in the gravity estimation and will permit better fault trending since the indicators are more correlated with the gravity of the fault.

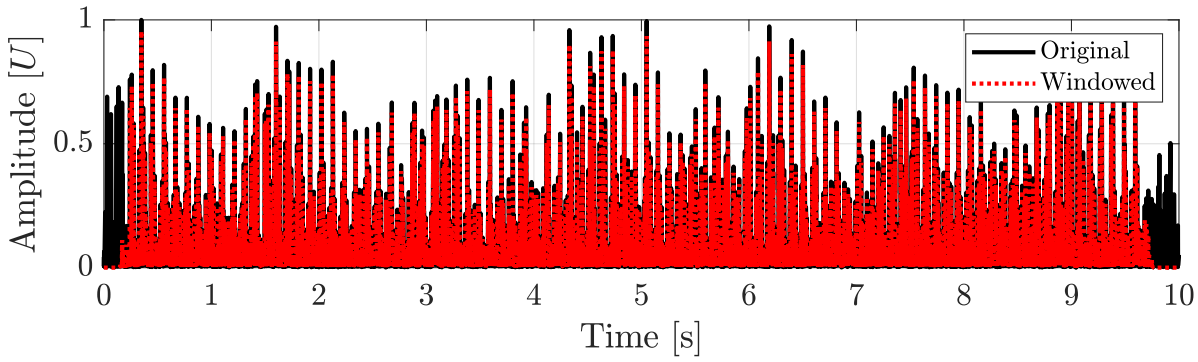


Figure 10: Envelope signal of day 75. The total signal is shown in dotted black line and the equivalent global windowed signal in red.

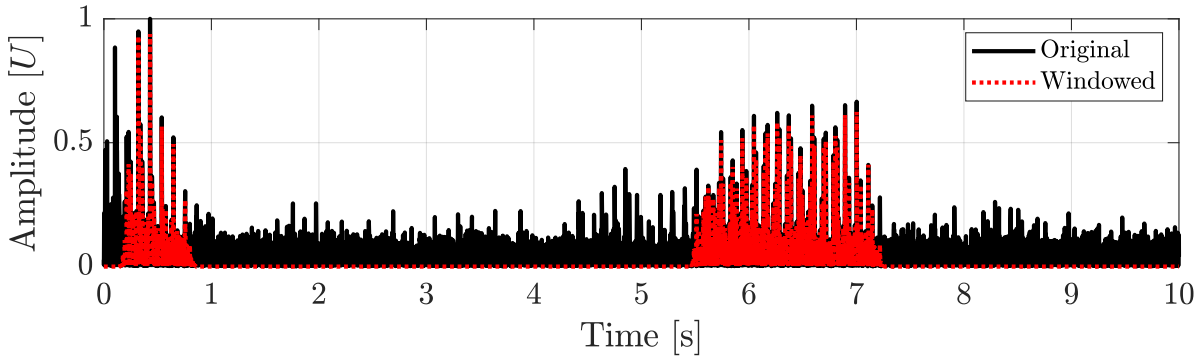


Figure 11: Envelope signal of day 77. The total signal is shown in dotted black line and the equivalent global windowed signal in red.

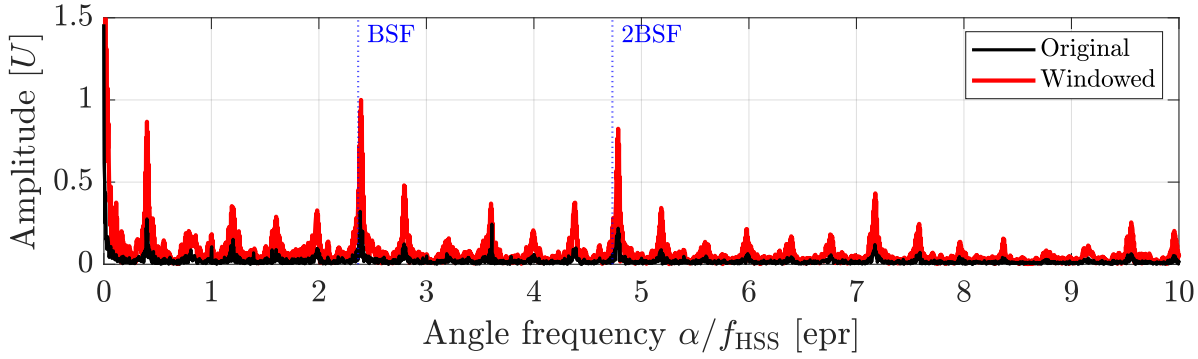


Figure 12: Fourier transform of the envelope signal of day 77 (black line) with Fourier transform weighed by the intermittency function (red line). The expected frequency for BSF is marked by the blue dotted lines.

## 6 Conclusion

A model of intermittent cyclostationary signal has been presented. This type of intermittent signal can model the vibrations generated by the flaked ball of a bearing. Scalar indicators for condition monitoring

assume a continuously and steadily observable phenomenon. The surveillance capacities of such indicators are degraded with a signal with intermittent signatures. An improved spectral indicator relying on the blind estimation of the intermittence function has been presented. The method was tested on the run-to-failure surveillance of a bearing of a wind turbine. This first approach to handling intermittent signals improved the gravity estimation of the fault. Further work will focus on the improvement of the method, mainly on the first ranking of segments and automatic selection.

# Appendix

## A Proof of proposition

The aim is to show that the sum of weighted versions of zero-padded Fourier transform of the windowed signal can be expressed like a global window as of Eq. (3). If a local window $g$ of length $M$ samples is slid along a signal $x$ of total length $N$ with overlapping of $O$ samples, the number of short-time segments along the signal is $I = (N - O)/(M - O)$. The relationship between index $n$ and $m$ the index of the window is $n = i(M - 0) + m$ with $m \in [0; M - 1]$ and $i$ the index of the segment. To retain the phase during the procedure, the overall $i^{th}$ window $v_i[n]$ applied to the signal has a value of zero on every bin except for an on-the-shelf local window $g[m]$ centred on sample $i(M - O) + m/2$, that is

$$v_i[n] = \begin{cases} g[m], & \text{if } n \in [i(M-O); i(M-O) + M - 1] \\ 0, & \text{else.} \end{cases} \tag{5}$$

The discrete Fourier transform is calculated for each windowed version of the signal. The retained spectrum is a weighed version of these spectra where the weight $u_i$ is given at the $i^{th}$ segment.

$$X(f) = \frac{1}{\sum_i u_i} \sum_{i=0}^{I-1} \frac{u_i}{\sum_n v[n]} \sum_{n=0}^{N-1} v_i[n] x[n] e^{-j2\pi n \frac{f}{F_s}} \tag{6}$$

where the equivalence with Eq. (3) is given by

$$\frac{w[n]}{\sum_n w[n]} = \sum_{i=0}^{I-1} \frac{u_i v_i[n]}{\sum_i u_i \sum_m g[m]}. \tag{7}$$

# References


[1] D.-Y. Kim, H.-B. Yun, S.-M. Yang, W.-T. Kim, and D.-P. Hong, "Fault diagnosis of ball bearings within rotational machines using the infrared thermography method," *Journal of the Korean Society for Nondestructive Testing*, vol. 30, no. 6, pp. 558–563, 2010, publisher: The Korean Society for Nondestructive Testing.

[2] J. M. Wakiru, L. Pintelon, P. N. Muchiri, and P. K. Chemweno, "A review on lubricant condition monitoring information analysis for maintenance decision support," *Mechanical Systems and Signal Processing*, vol. 118, pp. 108–132, Mar. 2019. [Online]. Available: https://linkinghub.elsevier.com/retrieve/pii/S0888327018305788

[3] M. Cerrada, R.-V. Sánchez, C. Li, F. Pacheco, D. Cabrera, J. Valente de Oliveira, and R. E. Vásquez, "A review on data-driven fault severity assessment in rolling bearings," *Mechanical Systems and Signal Processing*, vol. 99, pp. 169–196, Jan. 2018. [Online]. Available: https://www.sciencedirect.com/science/article/pii/S0888327017303242

[4] J. Antoni, F. Bonnardot, A. Raad, and M. El Badaoui, "Cyclostationary modelling of rotating machine vibration signals," *Mechanical Systems and Signal Processing*, vol. 18, no. 6, pp. 1285–1314, Nov. 2004. [Online]. Available: https://linkinghub.elsevier.com/retrieve/pii/S0888327003000888

[5] D. Abboud, J. Antoni, M. Eltabach, and S. Sieg-Zieba, "Angletime cyclostationarity for the analysis of rolling element bearing vibrations," *Measurement*, vol. 75, pp. 29–39, Nov. 2015. [Online]. Available: https://www.sciencedirect.com/science/article/pii/S0263224115003528

[6] J. Antoni, "Cyclic spectral analysis of rolling-element bearing signals: Facts and fictions," *Journal of Sound and Vibration*, vol. 304, no. 3-5, pp. 497–529, Jul. 2007. [Online]. Available: https://linkinghub.elsevier.com/retrieve/pii/S0022460X07001551

[7] J. Zhu, T. Nostrand, C. Spiegel, and B. Morton, "Survey of Condition Indicators for Condition Monitoring Systems," *Annual Conference of the PHM Society*, vol. 6, no. 1, 2014, number: 1. [Online]. Available: http://www.papers.phmsociety.org/index.php/phmconf/article/view/2514

[8] I. Howard, "A Review of Rolling Element Bearing Vibration 'Detection, Diagnosis and Prognosis',," DEFENCE SCIENCE AND TECHNOLOGY ORGANIZATION CANBERRA (AUSTRALIA), Tech. Rep., Oct. 1994, section: Technical Reports. [Online]. Available: https://apps.dtic.mil/sti/citations/ADA291123

[9] R. B. Randall and J. Antoni, "Rolling element bearing diagnostics—A tutorial," *Mechanical Systems and Signal Processing*, vol. 25, no. 2, pp. 485–520, Feb. 2011. [Online]. Available: https://www.sciencedirect.com/science/article/pii/S0888327010002530

[10] E. P. Kingsbury, "Ball Contact Locus in an Angular Contact Bearing," *Journal of Lubrication Technology*, vol. 105, no. 2, pp. 166–170, Apr. 1983. [Online]. Available: https://asmedigitalcollection.asme.org/tribology/article/105/2/166/422601/Ball-Contact-Locus-in-an-Angular-Contact-Bearing

[11] H. Xi, T. R. Lin, F. Wang, Y. Zhou, G. Wang, and P. Liu, "Contact probabilities of an angular ball bearing under a combined axial and radial load," *Mechanism and Machine Theory*, vol. 157, p. 104196, Mar. 2021. [Online]. Available: https://linkinghub.elsevier.com/retrieve/pii/S0094114X20304134

[12] P. Smaragdis, B. Raj, and M. Shashanka, "A probabilistic latent variable model for acoustic modeling," *Advances in models for acoustic processing, NIPS*, vol. 148, pp. 8–1, 2006, publisher: Citeseer.

[13] M. N. Schmidt and J. Larsen, "Reduction of non-stationary noise using a non-negative latent variable decomposition," in *2008 IEEE Workshop on Machine Learning for Signal Processing*. Cancun, Mexico: IEEE, Oct. 2008, pp. 486–491. [Online]. Available: http://ieeexplore.ieee.org/document/4685528/

[14] Y. Hao, L. Song, M. Wang, L. Cui, and H. Wang, "Underdetermined Source Separation of Bearing Faults Based on Optimized Intrinsic Characteristic-Scale Decomposition and Local Non-Negative Matrix Factorization," *IEEE Access*, vol. 7, pp. 11 427–11 435, 2019. [Online]. Available: https://ieeexplore.ieee.org/document/8610086/

[15] J. Sokołowski, J. Obuchowski, A. Wyłomańska, P. Kruczek, and R. Zimroz, "Multiple local damage detection method based on time-frequency representation and agglomerative hierarchical clustering of temporary spectral content," *Applied Acoustics*, vol. 147, pp. 44–55, Apr. 2019. [Online]. Available: https://linkinghub.elsevier.com/retrieve/pii/S0003682X17306977

[16] G. Xin, N. Hamzaoui, and J. Antoni, "Semi-automated diagnosis of bearing faults based on a hidden Markov model of the vibration signals," *Measurement*, vol. 127, pp. 141–166, Oct. 2018. [Online]. Available: https://linkinghub.elsevier.com/retrieve/pii/S0263224118304299

[17] J. Antoni, "Fast computation of the kurtogram for the detection of transient faults," *Mechanical Systems and Signal Processing*, vol. 21, no. 1, pp. 108–124, Jan. 2007. [Online]. Available: https://www.sciencedirect.com/science/article/pii/S0888327005002414

[18] F. Bonnardot, M. El Badaoui, R. Randall, J. Danière, and F. Guillet, "Use of the acceleration signal of a gearbox in order to perform angular resampling (with limited speed fluctuation)," *Mechanical Systems and Signal Processing*, vol. 19, no. 4, pp. 766–785, Jul. 2005. [Online]. Available: https://linkinghub.elsevier.com/retrieve/pii/S0888327004000664